Journal of Inorganic and General Chemistry
ZAAC
Zeitschrift für anorganische und allgemeine Chemie
DOI: 10.1002/zaac.202000061
ARTICLE

Extracting $[Pd@Sn_9]^{4-}$ and $[Rh@Pb_9]^{4-}$ Clusters from their Binary Alloys Using "*Metal Scissors*"

Marina Boyko,[a] Viktor Hlukhyy,[a] Hanpeng Jin,[a] Jasmin Dums,[a] and Thomas F. Fässler*[a]

Dedicated to Professor Bernd Harbrecht on the Occasion of his 70th Birthday

Abstract. The search for novel ternary intermetallic compounds with specific structures is still a challenge. We found that the two-step synthesis giving a typical alloy in the first step followed by the reaction of this alloy with alkali metals is a promising route. The intermetallic compounds $K_{12}Pd_{0.47}Sn_{17}$ and K_4RhPb_9 were synthesized by high-temperature reactions of preformed Pd-Sn and Rh-Pb alloys with K acting as "*metal scissors*" and were characterized by means of single crystal and powder X-ray diffractometry. The salt-like ternary phases $K_{12}Pd_{0.47}Sn_{17}$ and K_4RhPb_9 contain novel endohedrally filled intermetalloid clusters $[Pd@Sn_9]^{4-}$ and $[Rh@Pb_9]^{4-}$, respectively. The crystal packing of the products corresponds to filled variants of the binary Zintl phases $K_{12}Sn_{17}$ and K_4Pb_9, respectively. The crystal structure of $K_{12}Pd_{0.47}Sn_{17}$ can be regarded as a hierarchical replacement variant of the hexagonal Laves phase $MgZn_2$, with $[Pd@Sn_9]^{4-}/[Sn_9]^{4-}$ and $[Sn_4]^{4-}$ on Mg and Zn positions, respectively, whereas the packing of $[Rh@Pb_9]^{4-}$ clusters in K_4RhPb_9 is *hcp*. $K_{12}Pd_{0.47}Sn_{17}$ was characterized by Raman spectroscopy. For the first time Raman modes typical for endohedrally filled $[Pd@Sn_9]^{4-}$ clusters are observed and in accordance with quantum-chemical calculations. In addition Raman spectroscopy shows also the presence of filled $Pd@Sn_9$ clusters in a phase of nominal composition "$Na_{12}Pd_2Sn_{17}$". The results are discussed with respect to the volume increase due the incorporation of transition metal atoms.

Introduction

Since the resemblance of homoatomic Zintl anions and the class of fullerenes[1–3] was first reported, several new endohedrally filled cages formed by Group 14 elements were discovered.[4–6] Various metal atoms with different radii can occupy these clusters, and the cluster unit itself can be modified simultaneously. It was suggested that tetrel (*E*) elements are especially capable to build larger clusters with deltahedral frameworks. Deltahedral clusters E_n are electron-precise species if the charge is –2. According to Wade's rules *closo*-E_n^{2-} species possess the required number of valence electrons 4n+2 (2n+2 skeleton electrons and 2n lone pairs), and thus the electron count is independent of n.[7,8] Prominent examples for E_n^{2-} are known for n = 6, 9 and 10. Larger clusters such as n = 12 are only formed in the presence of templating atoms, resulting in endohedrally filled clusters such as $[Ni@Pb_{10}]^{2-}$, $[Ir@Sn_{12}]^{2-}$ or $[Pd_2@Ge_{18}]^{2-}$.[9–11]

Nonetheless, most examples are known for the nine-atomic clusters which adapt a *nido*-structure and have a charge of –4.[7] Generally, these filled nine-atomic clusters are synthetized by the reaction of a solution of K_4E_9 with organometallic compounds in the presence of cryptands (e.g. [2.2.2]crypt), leading e.g. to the Cu^+-centered clusters $[Cu@E_9]^{3-}$ (*E* = Sn, Pb).[12,13]

In comparison to the large number of known endohedral clusters obtained from solution, there are only a few examples received by solid-state synthesis. Remarkable examples are $A_{12}Cu_{12}Sn_{21}$[14] (A = Na – Cs) and $Na_{2.8}Cu_5Sn_{5.6}$[15] with Sn-centered units in form of discrete $[Sn@Cu_{12}@Sn_{20}]^{12-}$ clusters and $^1_\infty[Sn_{0.6}@Cu_5@Sn_5]$ rods, respectively. Due to the high formal charge of the anion $[Sn@Cu_{12}@Sn_{20}]^{12-}$, and thus in contrast to the isosteric $[As@Ni_{12}@As_{20}]^{3-}$ and $[Sb@Pd_{12}@Sb_{20}]^{3-/4-}$ units with lower charges,[16] it exists only in the solid state and is not soluble.

Interestingly, there are a number of the Sn-rich intermetallic compounds of transition metals *T*-Sn (*T* = Ru, Rh, Pd, Os, Ir, and Pt), in which the transition metals are encapsulated by a framework of tin atom cages (Figure 1). The size and the number of vertices of these cages and thus the coordination number of the hosted transition metal atom depend on the *T* : Sn ratio. At a smaller *T* : Sn ratio of 2:3 six-atomic cages $[T@Sn_n]$ appear with the shape of distorted octahedra, whereas eight-atomic clusters are obtained as tetragonal prisms or antiprisms at *T*:Sn ratios of 1:2, 3:7, 1:3, and 1:4, and at higher ratios (4:17) nine-atomic cages are found. These coordination polyhedra are sharing edges and typically found in intermetallic compounds.

The similarity to the discrete endohedrally filled clusters obtained in solution is most obvious in Os_4Sn_{17}, where the $[Os@Sn_9]$ units solely share edges, and which might be transferred to discrete anionic clusters by the reduction with alkali metals; thus the alkali metals can be regarded as "*metal scis-*

* Prof. Dr. T. F. Fässler
E-Mail: Thomas.Faessler@lrz.tum.de
[a] Department of Chemistry
Technische Universität München
Lichtenbergstraße 4
85747 Garching, Germany
Supporting information for this article is available on the WWW under **http://dx.doi.org/10.1002/zaac.202000061** or from the author.

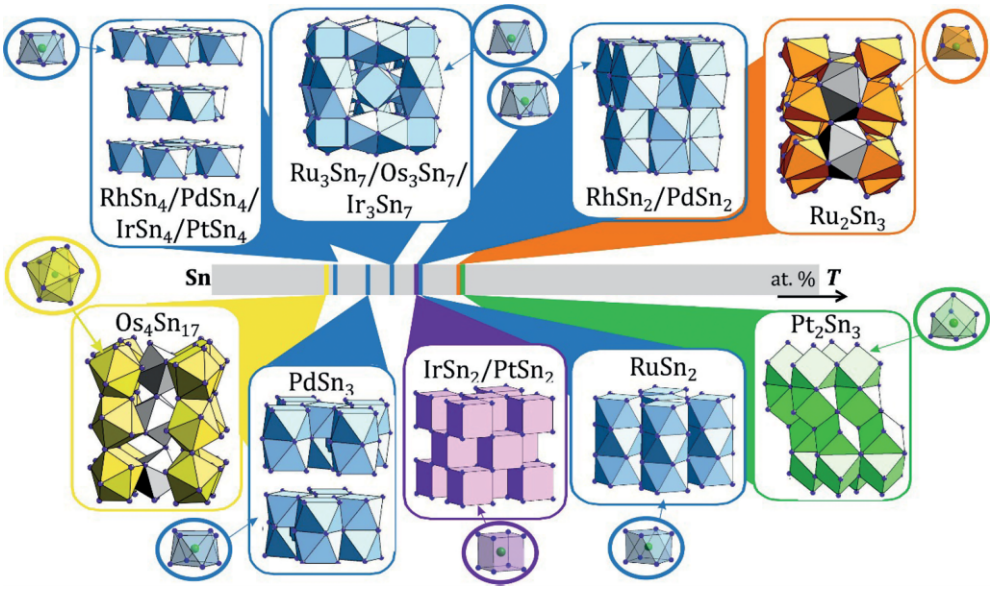

Figure 1. Sn-rich binary *T*-Sn (*T* = element of the Pt-group) phases are featuring *T* metals encapsulated in [Sn_n]-cages. [Sn_6]: distorted octahedron (orange); [Sn_7]: heptahedron (defective cube, green), [Sn_8]: square antiprism (blue), [Sn_8]: cube (violet), [Sn_9]: mono-capped square antiprism (yellow).

sors". The concept of *metal scissors* has already been applied successfully and allowed for the synthesis of endohedrally filled nine-atomic clusters via a solid state approach, resulting in the discrete anions $[Co@Sn_9]^{5-}$ in $K_{5-x}Co_{1-x}Sn_9$[17] and $K_{13}CoSn_{17}$[18] as well as $[Ni@Sn_9]^{4-}$ in $K_{12}Ni_{1-x}Sn_{17}$.[18]

We followed the two-step procedure by alloying first the *p*-block and transition metal and subsequent reaction with alkaline metal, which we had successfully introduced before.[14,15,17,18] We now investigated this approach for the Pd-Sn system with the predominant structural motif in $PdSn_3$ being a [Pd@Sn_8] cluster unit. We also studied Pb-containing alloys. K_4Pb_9 contains discrete $[Pb_9]^{4-}$ clusters,[19,20] and endohedrally filled clusters are only known from reactions in solution, with $[Cu@Pb_9]^{3-}$ [12] as the only representative so far. In the recently reported cluster units $[Ni@Pb_{10}]^{2-}$ and $[T@Pb_{12}]^{2-}$ (*T* = Ni, Pd, Pt) the *T* atoms are filling the larger bi-capped square antiprisms (CN = 10) and icosahedra (CN = 12), respectively.[9,21] The herein presented examples $K_{12}Pd_{0.47}Sn_{17}$ and K_4RhPb_9, which were synthesized by high-temperature reactions of preformed Pd-Sn and Rh-Pb alloys with potassium, contain for the first time filled cluster units $[Pd@Sn_9]^{4-}$ and $[Rh@Pb_9]^{4-}$, respectively, in the neat solids.

Experimental Section

Synthesis and Characterization: All manipulations were carried out under a purified argon atmosphere by using standard Schlenk and glove box techniques. The reactants were elemental K (Riedel-de-Haën, 99.9%), Pd (Aldrich, 99.9+%), Rh (ChemPur, 99.9%), Sn (ChemPur, 99.999%) and Pb (ABCR, 99.5%).

$K_{12}Pd_{0.47}Sn_{17}$: A ternary sample with a nominal composition K : Pd : Sn = 4 : 1 : 9 (58.7 mg of K, 40.0 mg Pd and 401.3 mg of Sn) was prepared in the high-temperature reaction of elemental potassium with a binary Pd-Sn precursor. An alloy of the nominal composition "$PdSn_9$" was synthesized by arc melting of the elements (water-cooled arc furnace, MAM-1, JOHANNA OTTO GmbH). Subsequently, pieces of K were added to the resulting "$PdSn_9$" regulus, and the mixture was packed into a tantalum crucible, which was welded-sealed on both sides under argon, jacketed in a fused silica Schlenk tube and evacuated to prevent oxidation of the crucibles at high temperatures. The Ta ampoule was hold at 960 and 600 °C for 12 and 48 h, respectively, in a resistance tube furnace (HTM Reetz LOBA 1200–40–600, Eurotherm 2416 controller) with slow cooling (0.1 K·min^{-1}) in between two steps and finally rapid cooling by quenching to room temperature. Powder X-ray phase analysis (Supporting Information, Figure S1) indicated that the main phase showed reflections rather similar to binary $K_{12}Sn_{17}$ along with the binary side-phase $PdSn_2$ plus some unindexed reflections. EDX analysis of selected crystals of the new phase (Supporting Information, Table S4) showed the presence of up to 5 at.% Pd, confirming the filling of the Sn_9 clusters with Pd, in agreement with the results of the single-crystal X-ray structure determination.

K_4RhPb_9: A ternary sample of the nominal composition K : Rh : Pb = 5 : 1.2 : 9 was prepared in a high-temperature reaction. First, a binary Rh–Pb precursor was prepared from elemental Rh and Pb in the ratio 1.2 : 9. For this, 341.6 mg of Pb powder and 22.6 mg of Rh powder were melted in an open niobium crucible under argon atmosphere using an induction furnace (Hüttinger Elektronik, Freiburg, Typ TIG 2.5/300). Then, 35.8 mg K was added, and the crucible was arc-sealed. The ampoule was placed in a silica tube, which was evacuated and inserted into a resistance tube furnace. The sample was heated to 1000 °C at a rate of 2 K min^{-1}, held at this temperature for 8 h, then slowly cooled to 650 °C at a rate of 0.1 K·min^{-1}, annealed at this temperature for 100 h and finally cooled rapidly by quenching to room temperature. An air-sensitive crystalline dark grey lustrous product was obtained from the reaction. The powder XRD diffractogram of the product (Figure S2, Supporting Information) shows the reflections of K_4RhPb_9 as the main phase, in accordance with the results of the single-crystal X-ray structure determination. In addition, another compound with a reflex pattern similar to that of $K_{12}Sn_{17}$, but with larger cell parameters is observed, which hints for a $K_{12}Rh_{1-x}Pb_{17}$ phase. It is worth to notice that a $K_{12}Pb_{17}$ phase has not been reported so far.

Powder X-ray Diffraction: For powder XRD analysis the samples were ground, diluted with diamond powder, and sealed in glass capillaries in an argon-filled glove box. Powder XRD data were collected with STOE STADI P powder diffractometer equipped with position-sensitive detectors (Mythen 1 K) using Cu-$K_{\alpha1}$ (λ = 1.54060 Å) or Mo-$K_{\alpha1}$ (λ = 0.70926 Å) radiation and curved Ge (111) monochromators. The STOE WINXPOW program package was used for phase analysis.[29]

Single Crystal X-ray Diffraction: A single crystal of $K_{12}Pd_{0.47}Sn_{17}$ was selected under perfluoropolyalkylether and mounted on top of a glass fiber, sealed in a glass capillary and measured on a Bruker D8 QUEST single-crystal X-ray diffractometer with PHOTON II CMOS Detector and IμS 3.0 Microfocus X-ray source (Mo-K_α) at 130 K. The frames were integrated with the Bruker SAINT software package[22,23] using a narrow-frame algorithm. Initially, the data set was indexed in the hexagonal symmetry, however, no acceptable structure solution could be implemented. A closer look into the diffraction data showed that the studied crystal is suffering from a multiple twinning: three domains were rotated by about 60° with respect to each other with a rotational axis along the pseudohexagonal direction [001]. Such pseudohexagonality of $A_{12}E_{17}$ or its filled variant is typical due to its structural relation to a Laves phase.[18,20] Integration of the diffraction data was performed with three orientation matrices with a ratio of 0.33:0.33:0.33 in a monoclinic unit cell (space group $P2_1/c$) with final cell parameters of a = 25.606(3), b = 14.815(2), c = 48.100(5) Å, β = 91.678(2)° and a volume V = 18238.68(4) Å^3. The integrated intensities for the reflections from the three components were written into a HKLF5 reflection file. Absorption correction was performed using SADABS.[24] The structure was solved and refined using the SHELXTL Software Package[25] in the monoclinic space group $P2_1/c$ (Z = 16) for the formula unit $K_{12.04(2)}Pd_{0.47(1)}Sn_{17}$. Significant disorder with split Sn positions within the tetrahedral clusters (positions Sn29-Sn36) and the nine-atomic clusters (positions Sn68-Sn77) as well as defect K positions with a partial occupancy of potassium (K46-K51) were found during the refinement. The positions of all four crystallographically independent Pd atoms filling the nine-atomic clusters are also partially occupied. Table 1 and Table S1 (Supporting Information) shows relevant crystallographic data and the conditions for the data collection and refinement procedures, and in Table S2 (Supporting Information) the atomic parameters and isotropic displacement parameters are listed. The diffractions are very weak due to large unit-cell parameters, poor crystal quality and significant structural disorder, which explains relatively high R factors. The highest residual electron density peak of 4.49 e·Å^{-3} in the difference Fourier map is located close to the Sn62 atom (ca. 1 Å), indicating further possible structural disorder.

A black irregular crystal of K_4RhPb_9 was selected under perfluoropolyalkylether and mounted on top of a glass fiber. Single-crystal intensity data were collected on an Oxford XCalibur3 diffractometer at 150 K. The Oxford CrysAlis RED software[26] was used for data processing, followed by numerical absorption correction with optimized crystal shapes using the X-SHAPE and X-RED programs.[27,28] On the basis of systematic extinctions, the structure was solved in the space group $P2_1/m$ by Direct Methods, using SHELXS-2014 and refined by employing the full-matrix least-squares procedure of SHELXL-2014 based on F^2.[29,30] Crystals of K_4RhPb_9 show only weak diffractions, owing to the poor crystal quality, which leads to high reliability factors. During the structure refinements several crystallographic problems occurred, which show a significant level of disorder within the [Rh@Pb_9] clusters. Reasonable split models could be used for these disordered clusters (Table S3, Supporting Information). The high residual electron density peaks in the difference Fourier maps are located close to the heavy Pb atoms of the clusters (ca. 1 Å), indicating further possible but less abundant disorder.

Table 1. Crystallographic data and selected details of structure refinement for $K_{12.04(2)}Pd_{0.47(1)}Sn_{17}$ and K_4RhPb_9.

	$K_{12.04(2)}Pd_{0.47(1)}Sn_{17}$	K_4RhPb_9
Formula weight /g·mol^{-1}	41224.1	2124.02
Space group	$P2_1/c$ (no. 14)	$P2_1/m$ (no. 11)
Z	16	4
Unit cell parameters:		
a /Å	25.606(3)	9.652(1)
b /Å	14.815(2)	13.462(1)
c /Å	48.100(5)	15.902(2)
β /deg	91.678(2)	102.69(1)
V /Å^3	18238.68(3)	2015.6(4)
Calculated density / g·cm^{-3}	3.697	6.999
Absorption coefficient (Mo-K_α) /mm^{-1}	10.412	76.461
F(000), e$^-$	17644	3436
Temperature, T /K	130	150
Θ range /deg	1.789–25.086	3.29–25.000
Reflections with $I > 2\,\sigma(I)$	21710 (R_6 = 0.0554)	2497 (R_6 = 0.0991)
Data / parameters	27536/1179	3695/161
GOF on F^2	1.067	1.093
Final R indices [$I>2\sigma(I)$]	R_1 = 0.0760, wR_2 = 0.2027	R_1 = 0.0998, wR_2 = 0.2468
Largest diff. peak and hole /e·Å^{-3}	4.485, –2.973	6.365, –3.073

Further details of the crystal structures investigations may be obtained from the Cambridge Crystallographic Data Centre, CCDC, 12 Union Road, Cambridge CB21EZ, UK (Fax: +44-1223-336-033; e-mail: deposit@ccdc.cam.ac.uk) and can be obtained free of charge on quoting the depository numbers CSD-1981652 and CSD-1981653.

EDX Measurements: After data collection the single crystals were analyzed by EDX measurements with a Jeol SEM 5900LV scanning electron microscope equipped with an Oxford Instruments INCA energy dispersive X-ray microanalysis system. No impurity elements heavier than sodium have been observed. A quantitative estimation of the atomic ratio was difficult due to the extreme air- and moisture-sensitivity of the material. Nevertheless, the analysis of the single crystals has revealed compositions, which are in agreement with the refined values within the standard deviations (Table S4, Supporting Information).

Raman Spectroscopy: Raman spectroscopy measurements were performed using a Renishaw inVia Raman microscope equipped with a CCD detector and laser (785 nm) with a maximum power of 500 mW. For operating the device, the software WiRe 4.2[31] was used. Samples were ground in an agate mortar inside of a glove box and then filled into glass capillaries (inner diameter 0.3 mm, wall thickness 0.01 mm, Hilgenberg GmbH), which were sealed using capillary wax (Hampton Research).

Computational Analysis: Computational analyses were performed using the Gaussian09 program package ,[32] with exchange correlation hybrid functional after Perdew, Burke and Ernzerhof (PBE0) and def2–TZVPP basis sets for all considered elements (Pd[33,34] and Sn[34,35]). A geometry optimization was carried out and the compensation of negative charges was carried out using a solvation model (polarizable continuum model, PCM).[36] J·mol,[37] VESTA 3,[38] IBOview[39] and OriginPro[40] were used for data processing and visualization. Calculated Raman lines were subject to change using appropriate scale factors.[41]

Supporting Information (see footnote on the first page of this article): Figures of powder X-ray diffractograms of "K_5PdSn_9", "$K_5Rh_{1.2}Pb_9$",

and "$Na_{12}Pd_2Sn_{17}$" samples; Figures of $[Sn_4]^{4-}$ and $[Pd@Sn_9]^{4-}$ clusters in $K_{12}Pd_{0.47}Sn_{17}$; Figure of $[Rh@Pb_9]^{4-}$ clusters in K_4RhPb_9; Table with results of the EDX analysis of $K_{12}Pd_{0.47}Sn_{17}$ and K_4RhPb_9 crystals; Table with crystal data and structure refinement for $K_{12}Pd_{0.47}Sn_{17}$ and K_4RhPb_9; Tables with coordinates and EDS for atoms of $K_{12}Pd_{0.47}Sn_{17}$ and K_4RhPb_9; Tables of hierarchical packing types of $[E_9]^{4-}$ and $[E_4]^{4-}$ clusters in $A_{12}E_{17}$ and A_4E_9 compounds; Table with calculated Raman data of $[Pd@Sn_9]^{4-}$ cluster.

Results and Discussion

Crystal Structure of $K_{12}Pd_{0.47}Sn_{17}$

The compound contains discrete tetrahedral Sn_4 and Sn_9 clusters. The latter are partially filled with Pd atoms, and the cluster units are separated by K atoms. The packing is closely related to that of other binary phases with an atomic ratio of 12 : 17. $K_{12}Pd_{0.47}Sn_{17}$ crystallizes in the monoclinic space group $P2_1/c$ and represents a filled variant of the parent α-$K_{12}Sn_{17}$ structure ($Rb_{12}Si_{17}$ structure type).[20,42] The increase of the unit cell volume correlates with the K atom content in the row $K_{12.04(2)}Pd_{0.47(1)}Sn_{17}$, $K_{12.92}Co_{0.95}Sn_{17}$, and $K_{13}CoSn_{17}$. An exception is the binary compound $K_{12}Sn_{17}$, which has probably been measured at higher temperature (Table 2).

The unit cell of $K_{12}Pd_{0.47}Sn_{17}$ (Figure 2) consists of eight crystallographically independent tetrahedral clusters $[Sn_4]^{4-}$ (4A, 4B, 4C, 4D, 4E, 4F, 4G, and 4H; Figure S4, Supporting Information) and four crystallographically independent nine-atomic clusters, which are centered by Pd atoms $[Pd@Sn_9]^{4-}$ (9A, 9B, 9C, and 9D; Figure S5, Supporting Information). The centers of the Sn_9 clusters of all four crystallographically independent sites are partially filled with Pd atoms with occupancies of 56(1) %, 54(1) %, 26(1) %, and 50(1) % for Pd1, Pd2, Pd3, and Pd4, respectively.

A special feature of $K_{12}Pd_{0.46}Sn_{17}$ is the disorder of one out of eight tetrahedra and of one out of four nine-atomic clusters. Both types of disorder are shown in Figure S5 (Supporting Information). The tetrahedra 4H can be interpreted as an overlay of the two tetrahedra $4H_1$ (Sn29, Sn30, Sn31, and Sn32) and $4H_2$ (Sn33, Sn34, Sn35, and Sn36) that occur with a ratio of 89.7(5) % : 10.3(5) %. The nona-cluster 9D is a combination of two clusters which share four atoms (Sn64, Sn65, Sn66, and Sn67) and five atoms with split positions $9D_1$ (Sn68, Sn69, Sn70, Sn71, and Sn72) and $9D_2$ (Sn73, Sn74, Sn75, Sn76, and Sn77) with ratio a ratio of 42.6(7) % : 57.4(7) %.

The nine-atomic clusters display two configurations (Figure 3c and d). On one hand, the atoms Pd1, Pd3 and Pd4 are surrounded by nine Sn atoms (clusters 9A, 9C, $9D_2$, respectively) forming a polyhedron with one rectangular face which could be regarded as a slightly deformed mono-capped square prism. On the other hand, Pd2 and Pd4 are encapsulated in the clusters 9B and $9D_1$, respectively, which are best described as tri-capped trigonal prisms with only trigonal faces.

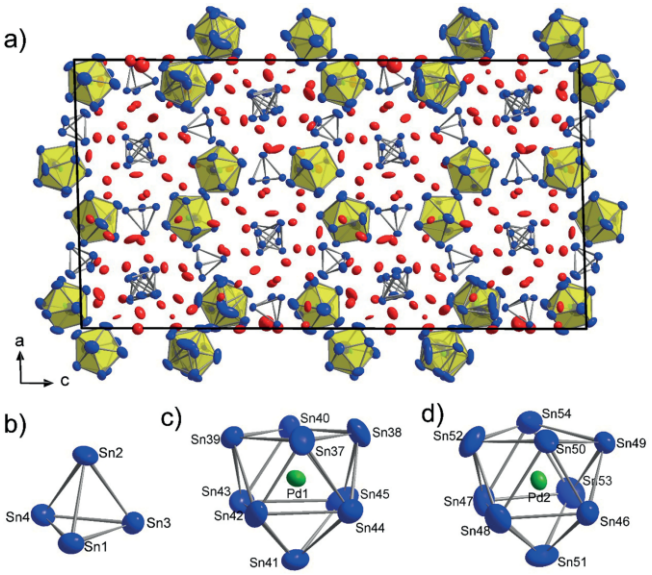

Figure 2. Crystal structure of $K_{12}Pd_{0.47}Sn_{17}$. (a) Unit cell, exemplary one (b) Sn_4 cluster, (c) $[Pd_{0.56}@Sn_9]^{4-}$ cluster with the shape of a distorted mono-capped antiprism, and (d) $[Pd_{0.54}@Sn_9]^{4-}$ cluster in the form of deformed tri-capped trigonal prism. All clusters are shown in Figure S6 (Supporting Information). Displacement ellipsoids are drawn at a 90 % probability level·K, Sn and Pd atoms are shown in red, blue and green, respectively.

In Table 3 selected interatomic distances are shown. The Sn–Sn distances of the $[Sn_4]^{4-}$ unit are in the range of 2.883(4)–2.986(4) Å and thus within the values found for K_4Sn_4 and $K_{52}Sn_{82}$.[43,44] The Sn–Sn distances in the $[Pd@Sn_9]^{4-}$ clusters lie between 2.786(8) and 3.505(4) Å, which is on average longer than those in the empty $[Sn_9]^{4-}$ clusters of K_4Sn_9 and $K_{52}Sn_{82}$. As expected the filling of the clusters with palladium atoms results in longer Sn–Sn distances and larger cluster volumes (Table 4) according to the calculation using the VESTA code.[38]

The volume increase of the ordered nine-atomic $[Pd@Sn_9]^{4-}$ unit compared to the empty $[Sn_9]^{4-}$ clusters amount to 11.1 % and 13.8 % for the species with approximate C_{4v} and D_{3h} sym-

Table 2. Unit cell parameters for the binary cluster compound $K_{12}Sn_{17}$ and its ternary derivatives containing $[Sn_9]$ clusters, endohedrally filled with transition metals.

Formula	Space group	Z	Unit cell parameters /Å			Volume /Å^3	T /K
			a	b	c		
$K_{12}Sn_{17}$ [43]	$P2_1/c$	16	25.71 β = 91.64°	14.77	48.19	18292.0	–
$K_{12.92}Co_{0.95}Sn_{17}$ [18]	$P2_1/n$	16	24.3661 β = 90.239°	25.7688	29.5949	18582.0	150
$K_{13}CoSn_{17}$ [18]	$Pbca$	16	26.1558	23.9928	29.7683	18681.1	150
$K_{12.04(2)}Pd_{0.47(1)}Sn_{17}$	$P2_1/c$	16	25.606(3) β = 91.678(2)°	14.815(2)	48.100(5)	18238.68(3)	130

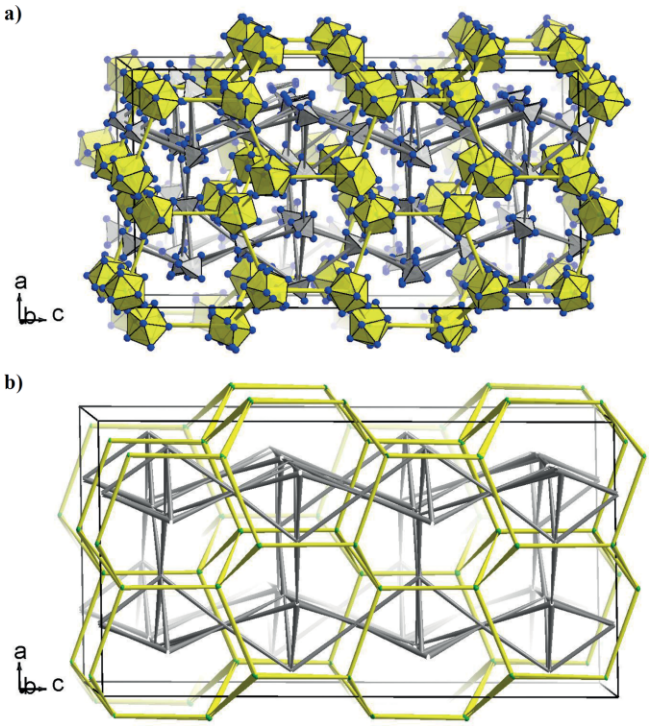

Figure 3. Representation of the anionic substructure within the structure of the $K_{12}Pd_{0.47}Sn_{17}$: $[Pd@Sn_9]^{4-}$ clusters in yellow and $[Sn_4]^{4-}$ units in grey (a) and the packing of the clusters showing relation to the $MgZn_2$-type (b).

metry respectively, which is in the range of other known $[T@Sn_9]^{n-}$ clusters (Table 4). We expected that the filling with the large Pd atoms should lead to an even stronger volume increase; however, since not all clusters are filled we observe an average size of filled and empty clusters.

$K_{12}Pd_{0.47}Sn_{17}$ shows a relatively low occupancy of the Pd atom sites inside the clusters (between 26 and 56 %), whereas the occupancy of the Co-centered $[Co@Sn_9]^{5-}$ clusters in $K_{5-x}Co_{1-x}Sn_9$ is higher with 76 to 82 %. In the Co- and Ni-centered $[T@Sn_9]^{4-/5-}$ clusters of $K_{12}Co_{1-x}Sn_{17}$ and $Na_{12}Ni_{1-x}Sn_{17}$, respectively, the occupancy is more than 93 %, and thus the largest volume increase found so far.

The Pd–Sn distances within the $[Pd@Sn_9]^{4-}$ cluster are between 2.470(1) and 2.806(1) Å, which is considerably shorter than those in certain binary Pd–Sn compounds. Notice, in the binary compounds the Sn atoms have a high coordination number arising in longer interatomic Sn–Sn distances: 2.788–2.837 Å for α-$PdSn_2$, 2.800–2.839 Å for β-$PdSn_2$, 2.805–2.810 Å for $PdSn_3$, and 2.750–2.814 Å for $PdSn_4$.

The cluster packing pattern in $K_{12}Pd_{0.46}Sn_{17}$ (similar to that of its parent structure α-$K_{12}Sn_{17}$) is a hierarchical variant of the hexagonal $MgZn_2$ structure type, where the $[Pd@Sn_9]^{4-}$ cluster is replaced by the Mg atom and the $[Sn_4]^{4-}$ clusters by Zn atoms (Figure 3). The larger $[Pd@Sn_9]$ clusters occupy the nodes of a hexagonal diamond-like network (yellow in Figure 3), whereas the smaller $[Sn_4]$ clusters are arranged alternately in 3^6 and 3.6.3.6 Kagomé nets (grey in Figure 3).

Table 3. Comparison of the *E*–*E* and *E*–*T* (*E* = Sn, Pb; *T* = transition metal) interatomic distances in empty and filled E_9 and Sn_4 clusters (in Å).

Compound	*d*(Sn–Sn) in $[Sn_9]^{4-}$	*d*(Sn–Sn) in $[Sn_4]^{4-}$	*d*(*T*–Sn) in $[T@Sn_9]^{n-}$
K_4Sn_4 [44]	–	2.947–2.955	–
K_4Sn_9 [45]	2.926–3.016	–	–
$K_{52}Sn_{82}$ [43]	2.510–3.682	2.804–2.996	–
$Na_{12}Ni_{1-x}Sn_{17}$ [18]	2.943–3.743	2.898–2.973	2.563–2.755
$K_{13}Co_{1-x}Sn_{17}$ [18]	2.964–3.457	2.893–2.951	2.563–2.680
$K_{12}Pd_{1-x}Sn_{17}$	2.786(8)–3.505(4)	2.883(4)–2.986(4)	2.470(1)–2.807(1)
	d(Pb–Pb) in $[Pb_9]^{4-}$		*d*(*T*–Sn) in $[T@Pb_9]^{n-}$
K_4Pb_9 [20]	2.950–3.431	–	–
$[K([2.2.2]crypt)]_3[Cu@Pb_9](dmf)_2$ [12]	3.132–3.294	–	2.708–2.802
K_4RhPb_9	2.973(5)–3.537(5)	–	2.624(7)–2.886(8)

Table 4. Cluster volumes of various ordered $[T@Sn_9]^{n-}$ units calculated with VESTA[46] and their relation to the empty $[Sn_9]^{4-}$ cluster.

Compound	Cluster	Approximate symmetry	Occupancy of *T* /%	Average cluster volume /Å^3	Volume increase /%
K_4Sn_9 [45]	$[Sn_9]^{4-}$	C_{4v}	0	33.4	–
$K_{52}Sn_{82}$ [43]	$[Sn_9]^{4-}$	C_{4v}	0	31.5	0
	$[Sn_9]^{4-}$	D_{3h}	0	31.8	0
$Na_{12}Ni_{1-x}Sn_{17}$ [18]	$[Ni1@Sn_9]^{4-}$	C_{4v}	95	36.1	14.6
	$[Ni2@Sn_9]^{4-}$	D_{3h}	93	36.2	13.8
$K_5Co_{1-x}Sn_9$ [17]	$[Co2@Sn_9]^{5-}$	C_{4v}	82	35.3	12.1
	$[Co1@Sn_9]^{5-}$	D_{3h}	80	35.4	11.3
	$[Co3@Sn_9]^{5-}$	D_{3h}	76	35.4	11.3
	$[Co4@Sn_9]^{5-}$	D_{3h}	79	35.4	11.3
$K_{13}Co_{1-x}Sn_{17}$ [18]	$[Co@Sn_9]^{5-}$	C_{4v}	100	36.1	14.6
$K_{12}Pd_{1-x}Sn_{17}$	$[Pd1@Sn_9]^{4-}$	C_{4v}	56	36.0	11.1
	$[Pd3@Sn_9]^{4-}$	C_{4v}	26	34.0	7.9
	$[Pd2@Sn_9]^{4-}$	D_{3h}	54	36.2	13.8

The lattice parameters a, b and c of $K_{12}Pd_{0.46}Sn_{17}$ and α-$K_{12}Sn_{17}$ are related to the hexagonal (sub)cell parameters a^* and c^* of a $MgZn_2$ Laves phase-type structure as $a = \sqrt{3} \times a^*$, $b = a^*$, $c = 2 \times c^*$. Since β-$K_{12}Sn_{17}$ represents the hierarchical variant of the cubic Laves phase $MgCu_2$,[20] one might expect also a corresponding packing of filled clusters which, however, has not been observed yet. Other known binary cluster compounds $A_{12}E_{17}$, which contain both $[E_9]^{4-}$ and $[E_4]^{4-}$ clusters, are mostly packed according to the $MgZn_2$ or $MgCu_2$ prototype after a hierarchical atom-to-cluster replacement (Table S5, Supporting Information).

Crystal Structure of K_4RhPb_9

K_4RhPb_9 crystallizes in the monoclinic space group $P2_1/c$ in a filled variant of the K_4Pb_9 structure. The structure consists of rhodium-filled $[Rh@Pb_9]^{4-}$ clusters, which are separated from each other by alkali metal K^+ counterions (Figure 4). The unit cell parameters of K_4RhPb_9 increase in all three directions compared to that of the binary K_4Pb_9, which leads to an expansion of the cell volume of about 3.3%. The unit cell of K_4RhPb_9 contains two crystallographically independent isolated cluster units [Rh1@Pb_9] and [Rh2@Pb_9] (Figure S6, Supporting Information). The clusters are separated, with a minimum vertex-to-vertex distances of 3.641(1) Å, similar to the separation in K_4Pb_9 with inter-cluster distances of 3.640 Å.[45]

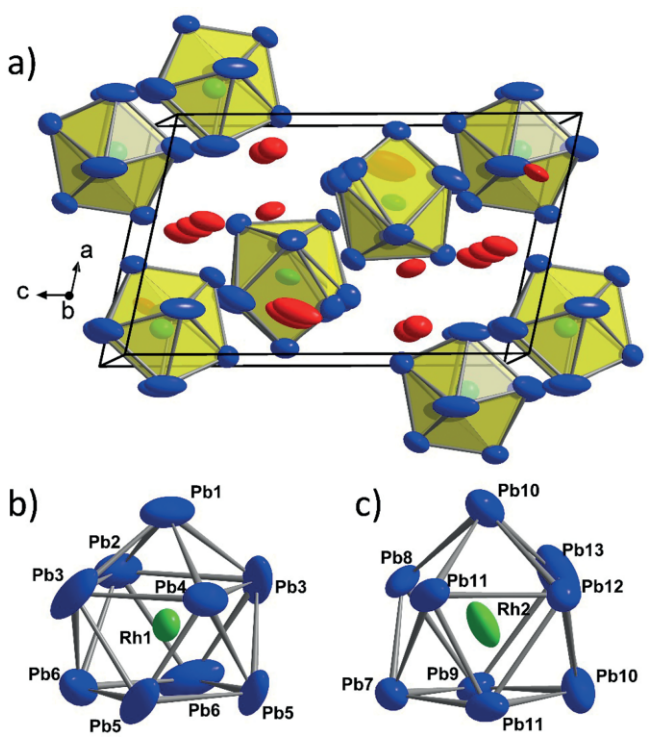

Figure 4. Crystal structure of the K_4RhPb_9: (a) unit cell; (b) and (c) two $[Rh@Pb_9]^{4-}$ clusters as representatives of overlaid clusters (for details see Figure S7, Supporting Information). K, Pb and Rh atoms are shown in red, blue and green color, respectively. Displacement ellipsoids are drawn at a 90% probability level.

As in the parent K_4Pb_9 structure, a significant level of disorder is observed in two crystallographically independent endohedrally filled nine-atomic [Rh@Pb_9] clusters of K_4RhPb_9, which is shown in Figure S7 (Supporting Information). Both clusters [Rh1@Pb_9] and [Rh2@Pb_9] can be described as an overlay of two clusters with equal ratios. All four clusters encapsulate the Rh1 and Rh2 atoms and adapt the shape of a C_{2v}-symmetric cluster best described as a tricapped trigonal prism in which two prism edges are elongated thus forming almost planar rectanglular faces that are capped by Pb atoms. By contrast, an only slightly distorted tri-capped trigonal prismatic cluster is found for the central Cu atom in the $[Cu@Pb_9]^{3-}$ cluster.[12]

The Pb–Pb distances within the Rh@Pb9 clusters [2.973(5)–3.537(5) Å] are slightly longer than those in the empty Pb_9 clusters in K_4Pb_9 (2.950–3.431Å). The Rh–Pb distances are within a range of 2.624(7)–2.886(8) Å, and some of them are shorter than the ones in the binary $RhPb_2$ compound, in which the Rh atoms have a square-antiprismatic coordination by Pb atoms [d(Rh–Pb) = 2.885 Å]. Further, the Rh@Pb_9 clusters are surrounded by 18 closest K^+ cations, similar to the empty Pb_9 clusters in K_4Pb_9. By contrast, the empty Sn_9^{4-} clusters in the binary phase K_4Sn_9 have only 16 closest K^+ cations. The shortest K–Pb distance is 3.45(2) Å, whereas for the parent phase K_4Pb_9 it is 3.50 Å.

In the structure of K_4RhPb_9 the Rh@Pb_9 clusters are arranged in a hierarchical variant of the hexagonal close packing (*hcp*), similar to that of the parent K_4Pb_9 structure. The hierarchical *hcp* and Cr_3Si packing are the two known hierarchical types in the binary A_4E_9 compounds (Table S6, Supporting Information). Interestingly, the hierarchical relationship to the *bcc* structure (body-centered cubic or W-type) with the Co@Sn_9 clusters at the W positions is observed for the $K_{5-x}Co_{1-x}Sn_9$ structure,[17] in which additional K^+ ions cause a less dense cluster packing with more octahedral voids for cations.

Raman Spectroscopy

It is known that the deltahedral clusters possess very characteristic Raman spectra.[20,47–50] We recently showed that endohedrally filled clusters show in contrast to the empty clusters a shift of the characteristic Raman lines of the empty clusters but also additional signals at higher wave numbers.[51] We found that Raman spectroscopy can also be applied for the Sn containing phases to show if filled clusters are present, in contrast to powder X-ray diffraction experiments that show too many reflections to determine changes in the cell parameters. The sample of the nominal composition "K_5PdSn_9" essentially contains the $K_{12}Pd_{0.47}Sn_{17}$ phase (Figure S1, Supporting Information) as deduced from single crystals. Thus Raman spectroscopy (Figure 5a) should give additional support on the presence of filled clusters. Additionally, a phase with a nominal composition of "$Na_{12}Pd_2Sn_{17}$" (Figure S3, Supporting Information) was examined by Raman spectroscopy.

Typical shifts of Raman bands for $K_{12}Sn_{17}$ have been reported by *H. G. von Schnering*[47] and the typical values appear

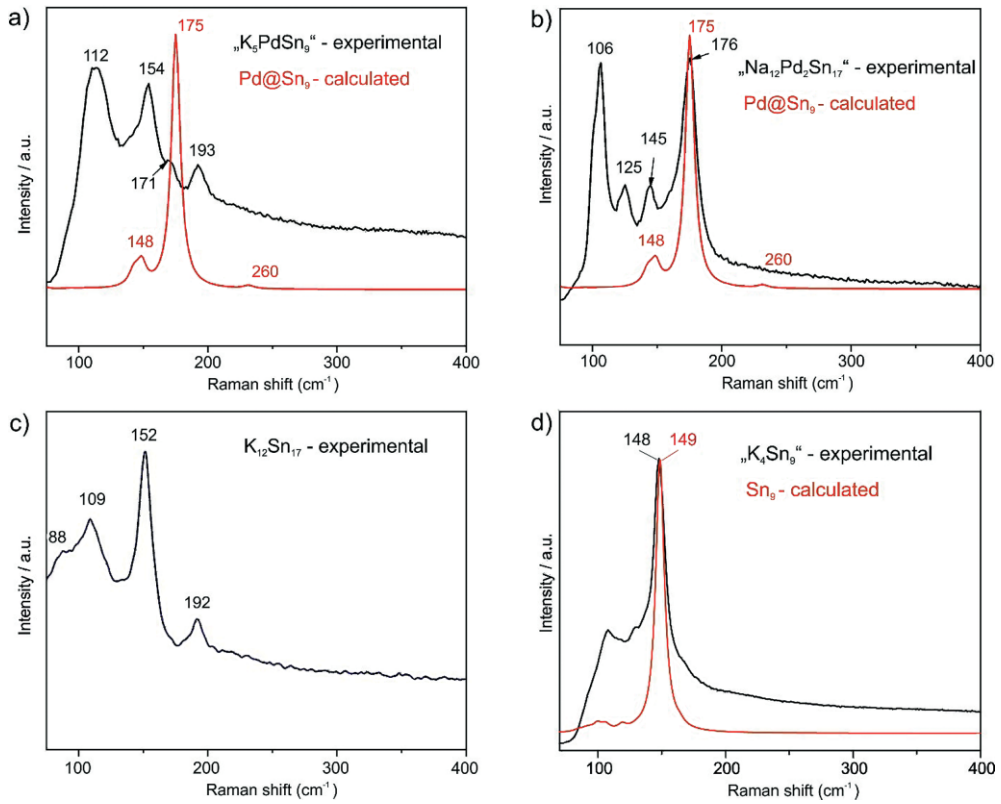

Figure 5. Experimental Raman spectra (black) of the samples: (a) "K_5PdSn_9", (b) "$Na_{12}Pd_2Sn_{17}$", (c) $K_{12}Sn_{17}$, and (d) K_4Sn_9 with calculated spectra for the respective $[Pd@Sn_9]^{4-}$ and $[Sn_9]^{4-}$ clusters (red). Intensity of Raman bands in arbitrary units.

at 93, 110, 152 (highest intensity), and 190 cm^{-1} and in good agreement with values measured on our instrument giving the following shifts: 88, 109, 152, and 192 cm^{-1} (Figure 5c). Data for K_4Sn_9 are available as well[47] and are shown in Figure 5d. The calculation of Raman spectra for this rather complex solid-state structures is currently not possible, therefore we include here calculated data obtained from molecular $[Sn_9]^{4-}$ clusters. The calculated spectrum is shown in Figure 4d and the strongest peak at 149 cm^{-1} is in good agreement with the experimental data of $K_{12}Sn_{17}$ and K_4Sn_9.

The Raman spectrum of $K_{12}Pd_{0.47}Sn_{17}$ ("K_5PdSn_9") shows the fingerprint of the $K_{12}Sn_{17}$ phase originating from the Sn_9 and Sn_4 cluster vibrations (Figure 5c and d). However, the additional signal at 171 cm^{-1} indicates the presence of also endohedrally filled clusters. This characteristic peak corresponds to the strongest signal according to the calculated Raman lines of $[Pd@Sn_9]^{4-}$.

Interestingly, this Raman band appears as strongest signal in the phase of the nominal composition "$Na_{12}Pd_2Sn_{17}$". Even though the structure of this phase could not be crystallographically determined and only a fingerprint-type powder diffractogram is available that hints for a 12:17 type phase (Figure S3, Supporting Information), the Raman signal at 175 cm^{-1} clearly shows the presence of $[Pd@Sn_9]^{4-}$ clusters.

Conclusions

We successfully applied a two-steps synthesis for the formation of novel intermetallic compounds comprising discrete endohedrally filled clusters. Alkali metals were used as "*alkali-metal scissors*" in a subsequent reaction step applied to a preformed alloy mixture. Even though single crystals suffer from disorder, the structure determination unequivocally revealed the presence of the novel filled clusters $[Pd@Sn_9]^{4-}$ and $[Rh@Pb_9]^{4-}$. In the case of the Sn containing phases the endohedrally filled clusters could also be detected by Raman spectroscopy. The spectroscopic results unambiguously allowed also the detection of filled clusters in phases of nominal composition such as "$Na_{12}Pd_2Sn_{17}$", whose structure could crystallographically not be determined.

Acknowledgements

Authors thank *Dr. Tobias Stürzer* (Bruker AXS GmbH) for single-crystal X-ray diffraction measurement.

Keywords: Intermetalloid cluster; Crystal structure; Intermetallic compound; Zintl anion

References

[1] T. F. Fässler, *Angew. Chem. Int. Ed.* **2001**, *40*, 4161–4165.
[2] T. F. Fässler, *Angew. Chem.* **2001**, *113*, 4289–4293.
[3] S. Frischhut, J. G. Machado de Carvalho, A. J. Karttunen, T. F. Fässler, *Z. Anorg. Allg. Chem.* **2018**, *644*, 1337–1343.
[4] S. Scharfe, T. F. Fässler, *Philos. T. Roy. Soc. A* **2010**, *368*, 1265–1284.

[5] C. Liu, Z.-M. Sun, *Coord. Chem. Rev.* **2019**, *382*, 32–56.
[6] R. J. Wilson, N. Lichtenberger, B. Weinert, S. Dehnen, *Chem. Rev.* **2019**, *119*, 8506–8554.
[7] K. Wade, in *Adv. Inorg. Chem. Radiochem., Vol. 18* (Eds.: H. J. Emeléus, A. G. Sharpe), Academic Press, **1976**, pp. 1–66.
[8] T. F. Fässler, S. D. Hoffmann, *Angew. Chem. Int. Ed.* **2004**, *43*, 6242–6247.
[9] E. N. Esenturk, J. Fettinger, B. Eichhorn, *Chem. Commun.* **2005**, 247–249.
[10] J.-Q. Wang, S. Stegmaier, B. Wahl, T. F. Fässler, *Chem. Eur. J.* **2010**, *16*, 1793–1798.
[11] J. M. Goicoechea, S. C. Sevov, *J. Am. Chem. Soc.* **2005**, *127*, 7676–7677.
[12] S. Scharfe, T. F. Fassler, S. Stegmaier, S. D. Hoffmann, K. Ruhland, *Chem. Eur. J.* **2008**, *14*, 4479–4483.
[13] S. Scharfe, F. Kraus, S. Stegmaier, A. Schier, T. F. Fässler, *Angew. Chem. Int. Ed.* **2011**, *50*, 3630–3670.
[14] S. Stegmaier, T. F. Fässler, *J. Am. Chem. Soc.* **2011**, *133*, 19758–19768.
[15] S. Stegmaier, T. F. Fässler, *Angew. Chem. Int. Ed.* **2012**, *51*, 2647–2650.
[16] Y. Wang, M. Moses-DeBusk, L. Stevens, J. Hu, P. Zavalij, K. Bowen, B. I. Dunlap, E. R. Glaser, B. Eichhorn, *J. Am. Chem. Soc.* **2017**, *139*, 619–622.
[17] V. Hlukhyy, H. He, L.-A. Jantke, T. F. Fässler, *Chem. Eur. J.* **2012**, *18*, 12000–12007.
[18] V. Hlukhyy, S. Stegmaier, L. van Wüllen, T. F. Fässler, *Chem. Eur. J.* **2014**, *20*, 12157–12164.
[19] V. Queneau, S. C. Sevov, *Inorg. Chem.* **1998**, *37*, 1358–1360.
[20] C. Hoch, M. Wendorff, C. Röhr, *J. Alloys Compd.* **2003**, *361*, 206–221.
[21] E. N. Esenturk, J. Fettinger, B. Eichhorn, *J. Am. Chem. Soc.* **2006**, *128*, 9178–9186.
[22] B. A. Inc., *APEX II Control Software*, Madison, Wisconsin, USA, **2012**.
[23] B. A. Inc., *SMART and SAINT*, Madison, Wisconsin, USA, **2012**.
[24] B. A. Inc., *SADABS*, Madison, Wisconsin, USA, **2001**.
[25] G. Sheldrick, *Acta Crystallogr., Sect. C: Cryst. Struct. Commun.* **2015**, *71*, 3–8.
[26] *CrysAlis RED*, CrysAlis RED, Version 1.171.33.34d ed., Oxford Diffraction Poland Sp. z o.o., **2009**.
[27] *X-SHAPE*, X-SHAPE Version 2.11 ed., STOE & Cie GmbH, Darmstadt (Germany), **2008**.
[28] *X-RED32*, X-RED32 Version 1.48 ed., STOE & Cie GmbH, Darmstadt (Germany), **2008**.
[29] G. M. Sheldrick, *SHELXL-2014 – Program for Crystal Structure Refinement*, University of Göttingen (Germany) **2014**.
[30] G. M. Sheldrick, SHELXS-2014 – Program for the Determination of Crystal Structure, University of Göttingen (Germany) **2014**.
[31] Renishaw, WiRE, Version 4.2 build 5037, **2002**.
[32] M. J. Frisch, G. W. Trucks, H. B. Schlegel, G. E. Scuseria, M. A. Robb, J. R. Cheeseman, G. Scalmani, V. Barone, B. Mennucci, G. A. Petersson, H. Nakatsuji, M. Caricato, X. Li, H. P. Hratchian, A. F. Izmaylov, J. Bloino, G. Zheng, J. L. Sonnenberg, M. Hada, M. Ehara, K. Toyota, R. Fukuda, J. Hasegawa, M. Ishida, T. Nakajima, Y. Honda, O. Kitao, H. Nakai, T. Vreven, J. A. Montgomery Jr., J. E. Peralta, F. Ogliaro, M. Bearpark, J. J. Heyd, E. Brothers, K. N. Kudin, V. N. Staroverov, T. Keith, R. Kobayashi, J. Normand, K. Raghavachari, A. Rendell, J. C. Burant, S. S. Iyengar, J. Tomasi, M. Cossi, N. Rega, J. M. Millam, M. Klene, J. E. Knox, J. B. Cross, V. Bakken, C. Adamo, J. Jaramillo, R. Gomperts, R. E. Stratmann, O. Yazyev, A. J. Austin, R. Cammi, C. Pomelli, J. W. Ochterski, R. L. Martin, K. Morokuma, V. G. Zakrzewski, G. A. Voth, P. Salvador, J. J. Dannenberg, S. Dapprich, A. D. Daniels, O. Farkas, J. B. Foresman, J. V. Ortiz, J. Cioslowski, F. D. J., *Gaussian09*, Wallingford CT, **2009**.
[33] D. Andrae, U. Häussermann, M. Dolg, H. Stoll, H. Preuss, *Theor. Chim. Acta* **1990**, *77*, 123.
[34] F. Weigend, R. Ahlrichs, *Phys. Chem. Chem. Phys.* **2005**, *7*, 3297–3305.
[35] B. Metz, H. Stoll, M. Dolg, *J. Chem. Phys.* **2000**, *113*, 2563.
[36] V. Barone, M. Cossi, *J. Phys. Chem. A* **1998**, *102*, 1995–2001.
[37] Jmol: an open-source Java viewer for chemical structures in 3D, http://www.jmol.org/.
[38] K. Momma, F. Izumi, *J. Appl. Crystallogr.* **2011**, *44*, 1272–1276.
[39] G. Knizia, J. E. M. N. Klein, *Angew. Chem. Int. Ed.* **2015**, *54*, 5518–5522.
[40] OriginLabCorp., *OriginPro, 9.3.226*, Northampton, MA, **2018**.
[41] M. L. Laury, M. J. Carlson, A. K. Wilson, *J. Comput. Chem.* **2012**, *33*, 2380–2387.
[42] V. Quéneau, E. Todorov, S. C. Sevov, *J. Am. Chem. Soc.* **1998**, *120*, 3263–3264.
[43] C. Hoch, M. Wendorff, C. Röhr, *Z. Anorg. Allg. Chem.* **2003**, *629*, 2391–2397.
[44] Y. Grin, M. Baitinger, R. Kniep, H. G. Von Schnering, *Z. Krist.-New Cryst. St.* **1999**, *214*, 453–454.
[45] C. Hoch, M. Wendorff, C. Rohr, *Acta Crystallogr., Sect. C* **2002**, *58*, I45–I46.
[46] K. Momma, F. Izumi, *J. Appl. Crystallogr.* **2011**, *44*, 1272–1276.
[47] H. G. Von Schnering, M. Baitinger, U. Bolle, W. Carrillo-Cabrera, J. Curda, Y. Grin, F. Heinemann, J. Llanos, K. Peters, A. Schmeding, M. Somer, *Z. Anorg. Allg. Chem.* **1997**, *623*, 1037–1039.
[48] W. Carrillo-Cabrera, R. Cardoso Gil, M. Somer, Ö. Persil, H. G. von Schnering, *Z. Anorg. Allg. Chem.* **2003**, *629*, 601–608.
[49] H. G. von Schnering, M. Somer, M. Kaupp, W. Carrillo-Cabrera, M. Baitinger, A. Schmeding, Y. Grin, *Angew. Chem.* **1998**, *110*, 2507–2509.
[50] L. J. Schiegerl, A. J. Karttunen, W. Klein, T. F. Fässler, *Chem. Sci.* **2019**, *10*, 9130–9139.
[51] B. J. L. Witzel, W. Klein, J. V. Dums, M. Boyko, T. F. Fässler, *Angew. Chem. Int. Ed.* **2019**, *58*, 12908–12913.

Received: February 12, 2020
Published Online: ■

Journal of Inorganic and General Chemistry
ZAAC
Zeitschrift für anorganische und allgemeine Chemie

ARTICLE